Joint Synchronization and Symbol Detection Design for Pulse-based Communications in the THz Band

Ajeya Gupta*, **Michael Medley**† and **Josep Miquel Jornet***

*Department of Electrical Engineering, University at Buffalo, The State University of New York, Buffalo, New York 14260, USA, E-mail: {ajeyayog,jmjornet}@buffalo.edu

†Air Force Research Laboratory/RITE, Rome, NY 13441, USA, Email: michael.medley@us.af.mil

***Abstract*—Ongoing research in graphene-based nano-transceivers and nano-antennas points to the Terahertz (THz) band (0.1–10 THz) as the communication frequency range for nano-devices. Femtosecond-long pulse-based modulation schemes have been proposed to enable ultra-broadband communication among nano-devices. One of the main challenges with ultra-high-speed pulse-based communications is the need for tight symbol synchronization between transmitter and receiver. In this paper, a synchronization scheme for pulse-based THz-band communications is designed and analyzed. The proposed scheme is aimed at iteratively estimating the symbol start time and reducing the observation window length for the symbol detector. The proposed scheme is fully analog and can be implemented with a combination of voltage-controlled delay (VCD) lines and Continuous-Time Moving-Average (CTMA) symbol detectors. Closed form expressions are obtained for the number of preamble symbols needed to achieve synchronization as well as the maximum number of bits that can be transmitted before requiring re-synchronization in the presence of clock skew. Similarly, the symbol error rate of the CTMA receiver is analytically modeled as a function of the resulting observation window length. Finally, the synchronization and symbol detection impact on the achievable throughput is studied. The developed scheme is experimentally tested with measured THz pulses and its performance is numerically investigated. The results show how the proposed scheme can successfully estimate the symbol start time and minimize the symbol error rate with less than ten synchronization preamble bits.**

I. Introduction

Nanotechnology is providing a new set of tools to the engineering community to control matter at the atomic and molecular scale. At this scale, novel nanomaterials show new properties that can be leveraged to develop new types of devices with unprecedented applications. For example, graphene [1], [2], a carbon-based two-dimensional material with advantageous physical, electrical and optical properties, can be used to develop miniature transceivers and antennas, just several hundreds of nanometers in size [3]–[6]. The very small size of these devices allows them to be embedded *anywhere*, and enables many new applications in the consumer, industrial, biomedical and military fields [7], such as nanosensor networks for chemical and biological attack prevention, or massive multi-core processing architectures on chip [8].

Ongoing research on graphene-based nano-transceivers and nano-antennas points to the Terahertz (THz) band (0.1–10 THz) as the communication frequency range for nano-devices [9], [10]. While molecular absorption introduces several challenges for long-range THz-band communication [11], [12], its impact is very low for distances below one meter, which is the expected communication distance of individual nano-devices. In this scenario, the THz-band behaves as a single transmission window which can support very large data rates, from multi-Gigabits-per-second (Gbps) to a few Terabits-per-second (Tbps). For example, in [13], it was shown that a simple communication scheme based on the transmission of one-hundred-femtosecond-long pulses can support wireless multi-Gbps and up to few Tbps links with ease.

One of the main challenges with ultra-high-speed pulse-based communications is the need for tight symbol synchronization between transmitter and receiver. Physical-layer synchronization affects the successful symbol detection probability and impacts the overall link performance. Unfortunately, we cannot directly reuse the existing solutions for similar pulse-based communication systems, such as Impulse-Radio Ultra Wide Band (IR-UWB) communications or Free Space Optical systems (FSO) [14]–[16]. One of the main reasons for this is the very short duration of THz pulses, which require the use of very high-speed Analog-to-Digital Converters (ADCs) for synchronization and symbol detection. The fastest existing ADC to date can only sample at rates below 100 Giga-Samples-per-second (GSas) [17], much below the Nyquist rate for THz signals. Furthermore, its size and power consumption make it inadequate for nano-devices. In addition to the lack of ADCs, the local clock [18] at different nano-devices might oscillate at slightly different frequencies, which can result in a significant clock skew between the transmitter and the receiver.

In this paper, we present a new synchronization scheme for pulse-based THz-band communication, which is based on dynamically time-shifting the signal at the receiver by means of a voltage-controlled delay (VCD) line [19] and adapting the observation window of a Continuous-Time Moving-Average

Acknowledgement of Support and Disclaimer: (a) The State University of New York at Buffalo acknowledges the U.S. Government's support in the publication of this paper. This material is based upon work funded by AFRL, under AFRL Grant No. FA8750-15-1-0050. (b) Any opinions, findings and conclusions or recommendations expressed in this material are those of the author(s) and do not necessarily reflect the views of AFRL.

Approved for Public Release; Distribution Unlimited: 88ABW-2015-2493.

(CTMA) symbol detector [20]. The fundamental idea is that, during an initial synchronization preamble, a synchronization block, which is composed by a bench of VCD lines and CTMA detectors, is used to iteratively determine the symbol start time and observation window length that is then used for the detection of the data symbols in the packet.

The main contributions of the paper are summarized as follows. We first describe and analyze the accuracy of the synchronization block and provide closed-form expressions for the number of bits in the preamble necessary to achieve synchronization, which depends on the number of elements in the synchronization block as well as the clock skew between transmitter and receiver (Sec. II). Then, we analyze the successful symbol detection probability of the CTMA symbol detector as a function of the observation window length determined from the synchronization block (Sec. III). In addition, we investigate the impact of the synchronization and symbol detection blocks on the achievable link throughput, and identify the optimal parameter values for their design (Sec. IV). Moreover, we validate and test the scheme with experimental data obtained with a THz time-domain spectroscopy platform, and provide extensive numerical results to support our developed solution (Sec. V). Finally, we conclude the paper in Sec. VI.

II. Time-delay-based Synchronization Scheme

A. System Model and Overview of the Proposed Solution

In our scenario, we consider that nodes communicate in an uncoordinated fashion and by utilizing a pulse-based time-spread on-off keying (TS-OOK) modulation. With TS-OOK, a logical zero is transmitted as silence, whereas a logical one is transmitted as a one-hundred-femtosecond-long pulse [13]. In addition, the time between symbols T_s is much longer than the symbol duration T_p, $\beta = T_s/T_p \gg 1$. Due to the low transmission power of nano-devices and the high path-loss at THz-band frequencies, the detection of such pulses is very challenging. Ideally, if the position of the pulse T_p within the symbol time T_s is known, the symbol detection probability can be maximized by shrinking the symbol detector observation window from T_s to T_p. However, it is not easy for the receiver to know the exact position of the pulse in advance.

The main objective of our proposed synchronization scheme is to jointly determine the symbol start time and the observation window length, by successively narrowing down the integration window around the true location of the pulse. More specifically, we consider that each packet incorporates a synchronization preamble composed of a pre-established sequence of logical zeros and ones. During the preamble, the synchronization block iteratively adapts the delay of the pulses at the receiver by means of a VCD line, which could be implemented for example by means of a graphene-based plasmonic waveguide [19]. The working principle of this VCD is based on the property that the propagation speed of a Surface Plasmon Polariton (SPP) wave on a graphene waveguide can be dynamically changed by electrically modulating the Fermi energy of the graphene layer [21]. This result is leveraged in our proposed design to change the signal propagation delay between the antenna and the symbol detector. In our design, we consider a CTMA detector, which outperforms energy-based detectors in terms of sensitivity [20] (see Sec. III).

The proposed synchronization scheme, illustrated in Fig. 1, can be implemented with an array of VCD lines and CTMA detectors and a single control logic circuit. Next, we describe the iterative procedure by which the symbol start time and observation window length are jointly determined.

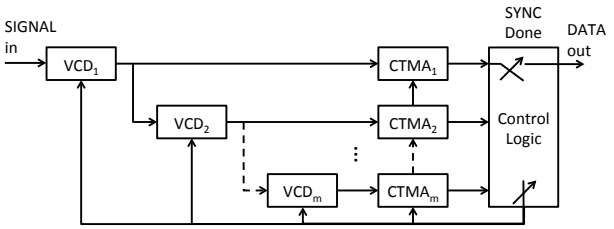

Fig. 1. Synchronization block diagram.

B. Symbol Start Time and Observation Window Length

Let m denote the number of channels or branches in the synchronization block shown in Fig. 1. Each branch is composed of a VCD line and a CTMA symbol detector, whose delay and observation window length, respectively, are dynamically adapted through the following iterative process.

Iteration 1: In the first iteration, the delay introduced by each VCD line is T_s/m and the CTMA observation window length is set to T_s/m. Together, all the CTMA detectors look for the pulse over the entire symbol time T_s. Based on this, the output of the first CTMA detector is equal to one only when the pulse is located between $[(m-1)T_s/m, Ts]$. Similarly, the output of the second CTMA detector is equal to one only when the pulse is located between $[(m-2)T_s/m, (m-1)T_s/m]$, and so on. The output of the last branch, m, is only equal to one when the pulse is located between $[0, T_s/m]$. We then define $block1$ as the block where the pulse is present.

Iteration 2: In this iteration, each CTMA detector utilizes an observation window of duration T_s/m^2. The first VCD line introduces a delay equal to $(block1-1)T_s/m + T_s/m^2$. The remaining VCD lines introduce a delay equal to T_s/m^2. Thus, the total delay in the second line is equal to $(block1-1)T_s/m + 2T_s/m^2$. Similarly, the total delay in the third line is equal to $(block1-1)T_s/m + 3T_s/m^2$, and so on. We then define $block2$ as the block where the pulse is found.

Iteration 3: In this iteration, each CTMA detector utilizes an observation window of duration T_s/m^3. The first VCD line introduces a delay equal to $(block1-1)T_s/m + (block2-1)T_s/m^2 + T_s/m^3$. The remaining VCD lines introduce a delay equal to T_s/m^3. Thus, the total delay in the second line is equal to $(block1-1)T_s/m + (block2-1)T_s/m^2 + 2T_s/m^3$. Similarly, the total delay in the third branch is equal to $(block1-1)T_s/m + (block2-1)T_s/m^2 + 3T_s/m^3$, and so on. We then define $block3$ as the block where the pulse is found.

Having explained the logic behind the first three iterations, we can write a generalized formula for the estimated symbol

start time T_d after the synchronization preamble:

$$T_d = \sum_{i=1}^{x-1} (block_i - 1)\frac{T_s}{m^i} + (block_x)\frac{T_s}{m^x}, \quad (1)$$

where m is the total number of branches in the synchronization block, x is the number of synchronization iterations and T_s is the symbol time. The maximum number of branches m is limited by the hardware constraints of nano-devices, and the number of iterations x depends on the length of the preamble bits sent by the transmitter. Both are considered parameter values in our analysis. Note there is no synchronization adjustment if the preamble bits are equal to zero.

Similarly, the observation window length T_{win} of the symbol detector after the synchronization preamble is given by

$$T_{win} = \frac{T_s}{m^x}, \quad (2)$$

and can also be written as a multiple of the pulse duration T_p

$$T_{win} = nT_p. \quad (3)$$

By combining (2) and (3), we can write n as

$$n = \frac{\beta}{m^x}, \quad (4)$$

where β is the spreading factor in TS-OOK.

From Fig. 1, once the synchronization phase is completed, we close the DATA out switch and disconnect the feedback to channels two to m. Hence, we can use the same block to capture the data by using only the first branch, with the VCD delay set to T_d and the observation window set to T_{win}.

C. Impact of Clock Skew

The clock skew, or difference between the transmitter and receiver clock frequencies, introduces further synchronization challenges. In particular, a mismatch in the symbol rates between the two nodes might progressively move the symbols outside of the detector observation window. This sets an upper bound on the number of data bits that can be transmitted before a new synchronization phase is needed. In this section, we investigate such bound for different values of the clock skew. In our analysis, we define the clock skew from the receiver's perspective. In particular, we consider that the symbol time T_s varies for each sample n at a rate μ

$$T_s[n] = T_s[n-1]\,(1+\mu)\,, \quad (5)$$

where μ can be either positive or negative. When μ is positive, the symbol period appears to increase with time, whereas when μ is negative, it appears to decrease.

Without loss of generality, we consider that, after the initial synchronization phase, the position p of the pulse within the observation window is characterized with a uniform random variable with probability density function (PDF) f_P given by

$$f_P(p) = \begin{cases} \frac{m^x}{T_s}, & \text{if } 0 < p < \frac{T_s}{m^x}, \\ 0, & \text{otherwise.} \end{cases} \quad (6)$$

Therefore, the expected pulse position is given by $\frac{T_s}{2m^x}$, or equivalently, $\frac{T_{win}}{2}$. The maximum number of bits n_{bits} to be transmitted before requiring a new synchronization phase is then computed as follows. When μ is positive, re-synchronization should happen before this condition is met

$$T_s[n] \geq T_s[0] + T_{win}/2 \quad (7)$$

where μ is the clock variation factor, T_s is the symbol time and T_p is the pulse time. By combining (7), (5) and (4), n_{bits} can be obtained as

$$T_s[0] \cdot (1+\mu)^{n_{bits}} = (T_s[0] + T_{win}/2), \quad (8)$$

$$n_{bits} = \frac{\log_{10}(1 + \frac{1}{2m^x})}{\log_{10}(1+\mu)}. \quad (9)$$

We can see that, as the value of μ increases, the number of bits after which re-synchronization should take place decreases, as expected. The same procedure can be followed to obtain the value of n_{bits} for $\mu < 0$, reaching the same equation for n_{bits} in (9), but with $|\mu|$ instead of μ.

III. Continuous-Time Moving-Average Detector

In this section, we describe and analytically model the performance of the CTMA symbol detector scheme, with a special emphasis on the impact of observation window T_{win} on the successful symbol detection probability.

A. Detector Overview

Traditional energy-based symbol detector schemes for pulse-based communication integrate the received signal over the entire symbol time or, following our definition, over the observation window T_{win}. The output is then compared to a pre-defined threshold and a decision on the received symbol is made. However, as mentioned before, the signals radiated by individual nano-devices have a very low power and are affected by the THz-band channel path-loss. This results into very high Symbol Error Rate (SERs) in realistic scenarios.

To overcome such limitation, a CTMA symbol detector for THz pulses was first proposed in [20]. A revised block diagram for the CTMA symbol detector is shown in Fig. 2.

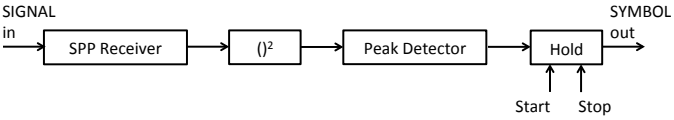

Fig. 2. CTMA symbol detector block diagram.

The fundamental idea behind this symbol detection scheme can be summarized as follows. When the detector integrates the pulse over a window T_{win} greater than the pulse time T_p, the noise contribution increases with T_{win}. This effect drops the performance of the receiver in terms of SER (Fig. 3(top)). To mitigate the impact of noise, we could reduce the integration time down to the pulse duration, T_p. However, since the observation window T_{win} is generally much larger than T_p, and we cannot know the exact position of the pulse within T_{win}, we would have to implement a total of T_{win}/T_p integrators in parallel and shifted in time to guarantee that the symbol is not missed. This implementation is certainly

impractical for low complexity devices. Additionally, the pulse may not perfectly fit in the integration time window (Fig. 3 (center)). Alternatively, we could just use a single integrator and move it in time at tiny steps $\Delta t \to 0$. This is the concept of a CTMA symbol detector (Fig. 3(bottom)).

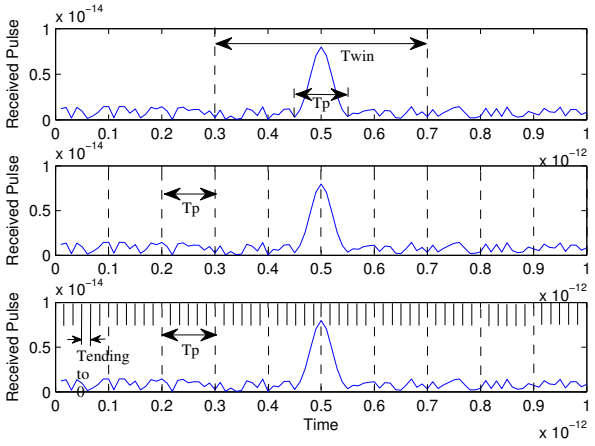

Fig. 3. Window length bigger than T_p (top); Window length equal to T_p, but pulse does not fit in a single integration window (center); Window length equal to T_p and pulse fits in a single integration window (bottom).

We define the CTMA detector as the linear time-invariant system with input to output relation given by

$$x(t) = \int_{t-T_p}^{t} v(t)\, dt, \tag{10}$$

where x stands for its output, t refers to time, T_p is the pulse time and v is the input signal to CTMA. As discussed in [20], the CTMA behaves as a low-pass filter and could be implemented with a discrete analog components. At each instant of time, the output of the CTMA, x is compared to a fixed threshold V_{th}, and the maximum value is held until the output is read and reset. The detector then decides whether the n-th symbol is one or zero according to:

$$s[n] = \begin{cases} 1, & \text{if } y = \max\{x(t)\} > V_{th}, \\ 0, & \text{otherwise}, \end{cases} \tag{11}$$

for $t \in [0, T_{win}]$. Next, we analytically investigate the successful symbol detection probability for both zeros and ones.

B. Detection of Zeros

In TS-OOK, zero is transmitted as silence and, thus, only noise is detected at the receiver side. For this, we consider the detected signal to be composed of N identically distributed random variables. We define $\boldsymbol{X} = \{X_1, X_2, ..., X_N\}$ as the vector that contains the N random variables and we use X_i to refer to the random variable that represents the value of the input signal x at time t_i. N depends on the observation window length, T_{win}, the integration window length of the CTMA, which we consider to be equal to T_p, and the time step of the CTMA detector, z. From (4), N can be written as

$$N = \frac{n-1}{z} + 1. \tag{12}$$

Strictly speaking, $z \to 0$, as the CTMA is an analog detector and, thus, $N \to \infty$. Then, from (11), the output of the symbol detector is given by $Y = \max\{\boldsymbol{X}\}$. Therefore, the PDF $f_{Y,no}$ of the output can be obtained as a function of the PDFs for the individual variables X_i. In particular, it follows that

$$f_{Y,no}(y) = \frac{d}{dy}(F_{no}(y))^N = NF_{no}(y)^{N-1} f_{no}(y), \tag{13}$$

where f_{no} and F_{no} stand for the PDF and the Cumulative Distribution Function (CDF) for each one of the individual random variables. From [22], we consider that each individual variable follows a chi-square distribution and, thus,

$$f_{no}(y) = \frac{y^{(v-2)/2} e^{-(y/2)}}{2^{y/2}\Gamma(\frac{y}{2})}, \tag{14}$$

where $y = 2X/N_0$ is the normalized signal with respect to the noise two-sided power spectral density N_0. $v = 2T_pB$ is the number of degrees of freedom, where T_p and B stand for the pulse duration and its equivalent bandwidth, and Γ refers to the Gamma function. Because we are using realistic THz pulses, which are further affected by the THz-band channel and the CTMA filter, the product T_pB is generally larger than one and, thus, there is no closed form solution for (13).

C. Detection of Ones

In TS-OOK, a logical one is transmitted as a one-hundred-femtosecond-long pulse. Following a similar methodology as before, we consider that the received signal is contributed by two kinds of random variables, some representing the pulse and some presenting noise. Hence, the output can be now represented as $Y = \max\{\boldsymbol{X}\} = \max\{\boldsymbol{X}_N, \boldsymbol{X}_S\}$, where $\boldsymbol{X}_N$ and $\boldsymbol{X}_S$ are vectors that contain N_n noise random variables and N_s signal random variables. As discussed in [20], provided that the signal power is kept higher than the noise power, $Y \approx \max\{\boldsymbol{X}_S\}$. Therefore, the PDF of the output $f_{Y,si}$ can be now written as

$$f_{Y,si}(y) = N_s F_{si}(y)^{N_s - 1} f_{si}(y), \tag{15}$$

where now each variable X_i is modeled as non-central chi-square distribution with

$$f_{si}(y) = \frac{1}{2}\left(\frac{y}{\lambda}\right)^{\frac{v-2}{2}} e^{\frac{-(y+\lambda)}{4}} I_{\frac{v-2}{2}}\left(\sqrt{y\lambda}\right), \tag{16}$$

where $\lambda = \frac{2E}{N_o} = v\ SNR$, $v = 2T_pB$, and I_n stands for the n-th order modified Bessel Function of the first kind. As before, there is no closed-form expression for (15).

D. Symbol Error Rate

To analyze the performance of the symbol detector as a function of the observation window length T_{win}, we are interested in computing the SER. This is directly obtained as

$$SER = P_{e|s=0} p_{s=0} + P_{e|s=1} p_{s=1}, \tag{17}$$

where p_0 and p_1 refer to the probability to transmit 0 and 1, respectively, and

$$P_{e|s=0} = \int_{\frac{2V_{th}}{N_0}}^{\infty} f_{Y,no}(y)\, dy, \tag{18}$$

$$P_{e|s=1} = \int_{0}^{\frac{2V_{th}}{N_0}} f_{Y,si}(y)\, dy, \tag{19}$$

where $f_{Y,no}$ and $f_{Y,si}$ are given by (13) and (15), respectively, and V_{th}/N_0 stands for the normalized signal power for the detection of logic 0 and logic 1 and N_0 stands for the noise level. The threshold value is calculated by finding out the intersection of logic 0 and logic 1.

IV. Throughput Analysis

From the discussion in Sec. III, we are interested in reducing the observation window length T_{win} to reduce the value of N in (13) and the SER given by (17). In Sec. II, we showed that with the proposed synchronization block, T_{win} can be reduced by increasing the number of synchronization bits x in (2). Transmitting longer preambles can result in a reduction of the throughput, but at the same, given that the SER is reduced, it is more likely that the transmitted bits are properly received, which improves the throughput. Therefore, there is a compromise between different parameter values on the synchronization and symbol detection block.

In this section, we aim at identifying the best values for such parameters, by defining the maximization of the throughput as an optimization problem. In particular, the problem is formulated as:

$$\begin{aligned}
&\text{Given:} && SNR, \mu \\
&\text{Find:} && m, x, n_{bits} \\
&\text{Maximize:} && S = \frac{n_{bits}}{T_{delay}} \\
&\text{Subject to:} && m^x \leq \beta; \quad n_{bits} \leq \frac{\log_{10}\left(1+\frac{1}{2\cdot m^x}\right)}{\log_{10}(1+|\mu|)}; \\
& && SER = \Psi(m, x, SNR); \\
& && FER = \Lambda(SER, n_{bits}, x); \quad \eta = 1/FER; \\
& && T_{delay} = (\eta - 1)(n_{bits} + P),
\end{aligned} \tag{20}$$

where

- The first constraint guarantees that the final observation window length T_{win} is shorter than the symbol duration T_s, as given by (4).
- The second constraint guarantees that there is no need for re-synchronization within the transmission of one frame. This depends on the clock skew μ in (9).
- Ψ in the third constraint represents the SER as a function of m, x and SNR, and is given by (17).
- Λ in the fourth constraint represents the Frame Error Rate (FER) and is a function of the SER and the total number of bits per frame, including the synchronization preamble. If we consider that a simple error detection scheme is used, without error correction capabilities,

$$\Lambda = (1 - SER)^{(n_{bits}+P)}, \tag{21}$$

where P is the total number of bits in the preamble, $P \geq x$, as not all the bits in the preamble might be ones.
- η refers to the average number of retransmissions per frame and T_{delay} refers to the average delay per frame.

The optimal values for m, x and n_{nits} that maximize the single link throughput can be then numerically obtained.

V. Experimental and Numerical Results

In this section, we first test the functioning of the proposed synchronization scheme with experimental THz pulses. Then, we numerically investigate the impact of different parameters on the performance of the synchronization and detection blocks and compute the achievable throughput.

A. Synchronization Test with Experimental Data

To test the functioning of the proposed synchronization algorithm, we utilize measured THz pulses generated and captured by means of a time-domain THz spectroscopy platform available to the authors. Such platform is able to generate one-hundred-femtosecond-long pulses, which are emitted in free space and measured at a distance by a detector. The captured signal is passed through the proposed synchronization block in Fig. 1 which iteratively estimates the symbol start time and, thus, the necessary delay to be introduced by the first VCD during the reception of the actual data symbols.

The different iterations of the algorithm for $m = x = 2$ are illustrated in Fig. 4. In the first iteration, CTMA_1 looks from $T_s/2$ to T_s and CTMA_2 looks from 0 to $T_s/2$. CTMA_2 detects the pulse and, thus, Block1=2. In the second iteration, CTMA_1 looks from $T_s/4$ to $T_s/2$ and CTMA_2 looks from 0 to $T_s/4$. Now CTMA_1 detects the pulse and, thus, Block2=1. During the data phase, VCD_1 is tuned to introduce a delay equal to $0.5T_s$ and CTMA_1 utilizes an observation window length equal to $T_s/4$. In Table I, we summarize the output for different number of pulses in the synchronization preamble x.

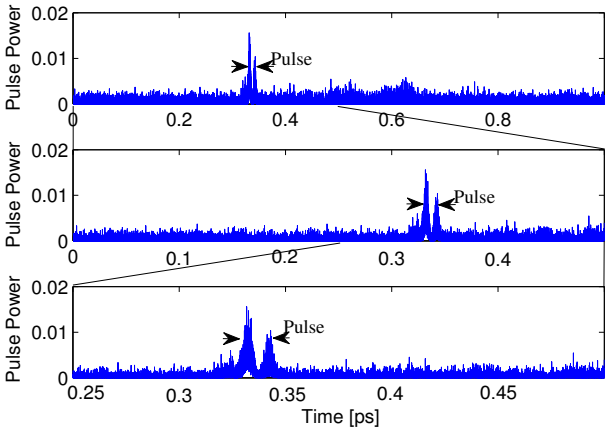

Fig. 4. Illustration of the synchronization algorithm for $m = x = 2$: First iteration (top); Second iteration (middle); Third iteration (bottom).

After the synchronization preamble, the measured data symbols were detected by utilizing the estimated delay for VCD_1 and the observation window length for CTMA_1. The

TABLE I
ITERATIONS IN THE SYNCHRONIZATION ALGORITHM (m=2)

Preamble	it=1	it=2	it=3	it=4	T_d	T_{win}
$x=2$	2	1	NA	NA	$3T_S/4$	$T_S/4$
$x=3$	2	1	2	NA	$3T_S/4$	$T_S/8$
$x=4$	2	1	2	1	$11T_S/16$	$T_S/16$

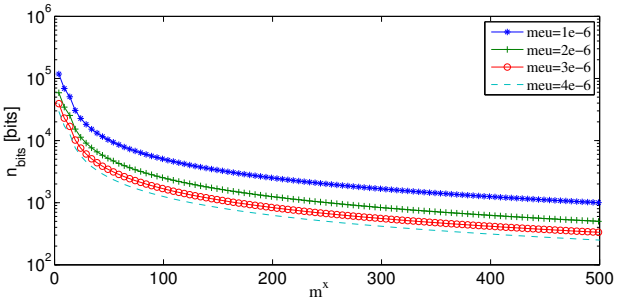

Fig. 5. Maximum number of bits before resynchronization as a function of m^x, for different values of the clock skew μ.

low noise in the measurements resulted in almost no symbol errors, in line with the numerical results discussed next.

B. Numerical Results

We consider the following parameters in our analysis. The transmitted pulses are modeled as the first time derivative of a Gaussian pulse with pulse length T_p=100 fs and pulse energy E_p=1 aJ. The time between symbols T_s is set to 10 ps ($\beta = 100$). Symbols are considered equiprobable, i.e., $p_{s=0} = p_{s=1} = 0.5$ in (17).

1) Impact of Clock Skew on the Frame Length: In Fig. 5, the number of bits n_{bits} after which resynchronization is needed given by (9) is shown as a function of number of branches in the synchronization block m, for different values of the clock skew μ. As expected, for higher values of μ, the number of bits after which re-synchronization should take place decreases hence signifying, re-synchronization becomes more often and more preamble bits are needed to transmit the same amount of data bits. Moreover, as the number of channel increases, the number of bits after which re-synchronization should take place decreases. This is because, T_{win} decreases as we increase m and hence, the CTMA looks to re-synchronize again when the clock shifts by a value of T_{win} which is small for large values of m.

2) Symbol Error Rate: In Fig. 6, the SER given by (17) is shown as a function of the SNR for four different values of m^x. As the term m^x increases, the observation window length T_{win} decreases and, thus, the SER also decreases. This can also be understood from the PDFs for the detected signal in the transmission of 0s and 1s, given by (13) and (15), respectively.

3) Throughput: In Fig. 7, the throughput given by (20) is plot as a function of the m^x for different values of the SNR. It can be seen that as the value of m^x increases, the throughput also increases. This result shows that the benefits of reducing SER by shortening the observation window length T_{win} largely overcome the cost introduced by increasing

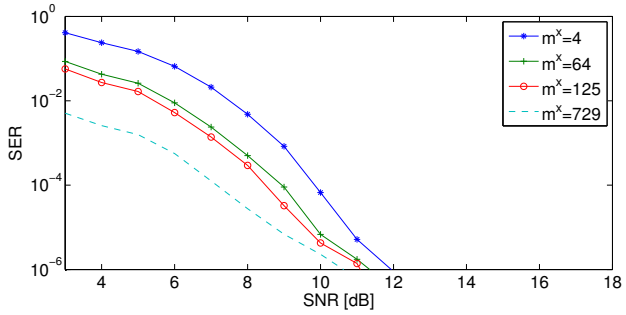

Fig. 6. SER as a function of the SNR for different values of m^x.

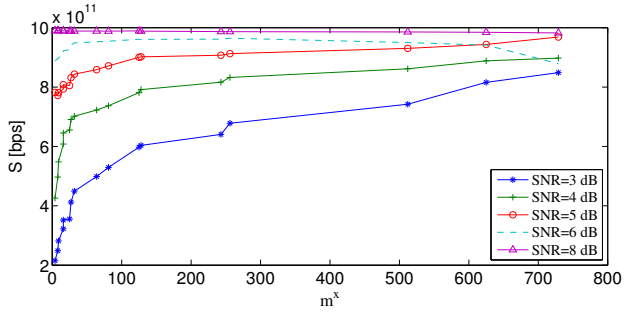

Fig. 7. Throughout as a function of the SNR for different values of m^x (frame length=1000 bits).

the size of the synchronization block, i.e., increasing m, or transmitting longer synchronization preambles, x.

Given the constraints of nano-devices, it seems more adequate to keep m to the minimum number possible, i.e., $m = 2$, and investigate the impact of x alone. In Fig. 8, the throughput is shown as a function of the x for $m = 2$. For low SNR values, the impact of x on the SER is larger than the impact of x in the total delay. Therefore, the throughput S increases rapidly with x at low values of SNR. For example, for SNR=3 dB, we can triple the throughput by adding only 6 bits to the synchronization preamble. For higher values of SNR, the impact of x on the SER is less significant and hence the throughput does not drastically change with x.

Finally, the impact of the number of bits per frame on the throughput S is illustrated by means of Fig. 9. For low values

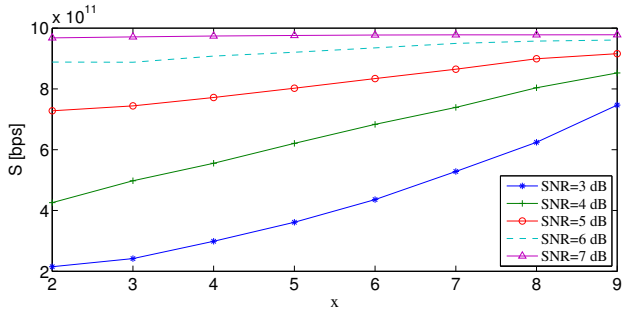

Fig. 8. Throughout as a function of the SNR for different values of x (m=2, frame length=1000 bits).

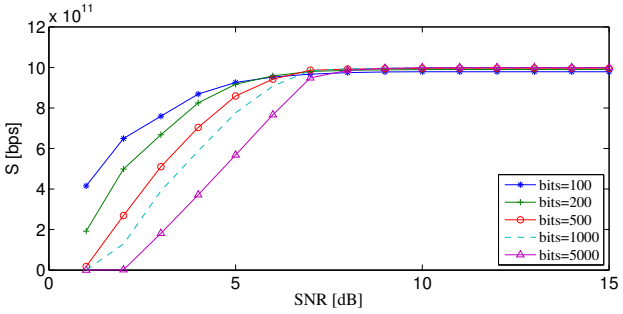

Fig. 9. Throughout as a function of the SNR for different values of $bits$ (m=3, x=6).

of SNR, lesser of bits should be sent in a single packet, whereas for large values of SNR, the trend reverses and the throughput remains the same for the different numbers of bits.

4) Optimal Synchronization and Detection Parameters: In light of the illustrated results, combined with exhaustive search, the values of m, n, SNR and $bits$ that are required to maximize the throughput can be summarized as follows. For SNR above 7 dB, the throughput remains almost constant for different values of x, m and $bits$. In that case, reducing m and x allows the transmission of longer frames, if needed, and simplifies the synchronization block hardware. Otherwise, the maximum throughput is numerically obtained for $x = 6$, $m = 3$ and $bits = 5000$. For low SNR values, significant improvement is achieved by increasing the number of bits in the synchronization preamble x. Maximum throughput is achieved again for $x = 6$ and $m = 3$, now with shorter frames.

VI. Conclusion

Recent progress in the field of nano-transceivers and nano-antennas points to the THz band as the frequency range of communication for novel nano-devices. In this paper, we have a proposed a joint physical-layer synchronization and symbol detection scheme for pulse-based THz-band communication. The main objective of the proposed scheme is to jointly determine the symbol start time and the observation window length, by successively narrowing down the integration window around the true location of the pulse. The proposed solution is fully analog and can be implemented with a combination of voltage-controlled delay lines and continuous-time moving-average symbol detectors with tunable observation window. We have analytically investigated the synchronization preamble length and the maximum number of bits to be transmitted before requiring re-synchronization. We have also obtained analytical expressions for symbol error rate as a function of the observation window length. We have investigated the compromise between synchronization preamble length and symbol detection observation window length, and investigated their joint impact on the achievable throughput. Finally, we have tested the algorithm with experimental THz pulses and provided extensive simulation results to analyze the impact of different parameters. The results show how, with the proposed synchronization algorithm, tight synchronization and low symbol error rates are possible just with very short preambles, less than bits long.

References

[1] A. K. Geim and K. S. Novoselov, "The rise of graphene," *Nature Materials*, vol. 6, no. 3, pp. 183–191, Mar. 2007.

[2] A. C. Ferrari, F. Bonaccorso, V. Fal'ko, K. S. Novoselov *et al.*, "Science and technology roadmap for graphene, related two-dimensional crystals, and hybrid systems," *Nanoscale*, vol. 7, pp. 4598–4810, 2015.

[3] J. M. Jornet and I. F. Akyildiz, "Graphene-based plasmonic nano-antenna for terahertz band communication in nanonetworks," *IEEE JSAC, Special Issue on Emerging Technologies for Communications*, vol. 12, no. 12, pp. 685–694, Dec. 2013.

[4] M. Tamagnone, J. Gomez-Diaz, J. R. Mosig, and J. Perruisseau-Carrier, "Reconfigurable terahertz plasmonic antenna concept using a graphene stack," *Applied Physics Letters*, vol. 101, no. 21, p. 214102, 2012.

[5] J. M. Jornet and I. F. Akyildiz, "Graphene-based plasmonic nano-transceiver for terahertz band communication," in *Proc. of European Conference on Antennas and Propagation (EuCAP)*, 2014.

[6] A. Cabellos-Aparicio, I. Llatser, E. Alarcon, A. Hsu, and T. Palacios, "Use of thz photoconductive sources to characterize tunable graphene rf plasmonic antennas," *IEEE Transactions on Nanotechnology*, vol. -, no. -, pp. –, 2015.

[7] I. F. Akyildiz and J. M. Jornet, "The internet of nano-things," *IEEE Wireless Communications Magazine*, vol. 17, no. 6, pp. 58–63, Dec. 2010.

[8] S. Abadal, E. Alarcon, A. Cabellos-Aparicio, M. Lemme, and M. Nemirovsky, "Graphene-enabled wireless communication for massive multicore architectures," *IEEE Communications Magazine*, vol. 51, no. 11, pp. 137–143, 2013.

[9] I. F. Akyildiz, J. M. Jornet, and C. Han, "Terahertz band: Next frontier for wireless communications," *Physical Communication (Elsevier) Journal*, vol. 12, pp. 16 – 32, Sep. 2014.

[10] H.-J. Song and T. Nagatsuma, "Present and future of terahertz communications," *IEEE Transactions on Terahertz Science and Technology*, vol. 1, no. 1, pp. 256–263, 2011.

[11] J. M. Jornet and I. F. Akyildiz, "Channel modeling and capacity analysis of electromagnetic wireless nanonetworks in the terahertz band," *IEEE Transactions on Wireless Communications*, vol. 10, no. 10, pp. 3211–3221, Oct. 2011.

[12] S. Priebe and T. Kurner, "Stochastic modeling of thz indoor radio channels," *IEEE Transactions on Wireless Communications*, vol. 12, no. 9, pp. 4445–4455, 2013.

[13] J. M. Jornet and I. F. Akyildiz, "Femtosecond-long pulse-based modulation for terahertz band communication in nanonetworks," *IEEE Transactions on Communications*, vol. 62, no. 5, pp. 1742 – 1754, May 2014.

[14] R. Merz, M. Flury, and J.-V. L. Boudec, "Synchronization for impulse-radio uwb with energy detection and multi-user interface: Algorithms and applications to ieee 802.15.4a," *IEEE Transactions on Signal Processing*, vol. 59, no. 11, pp. 5458–5472, Nov. 2011.

[15] R. Akbar, S. A. Emanuel Radoi, and M. N. ul Islam, "Low complexity synchronization algorithms for orthogonally modulated ir-uwb systems," *EURASIP Journal on Wireless Communications and Networking*, 2013.

[16] X. Y. Wang and A. B. Apsel, "Pulse coupled oscillator synchronization for low power uwb wireless transceivers," in *50th IEEE Midwest Symposium on Circuits and Systems (MWSCAS)*, 2007, pp. 1524–1527.

[17] Fujitsu. 56GSa/s 8-bit Analog-to-Digital Converter. [Online]. Available: http://www.fujitsu.com/us/Images/56G_ADC_FactSheet.pdf

[18] F. Rana, "Graphene terahertz plasmon oscillators," *IEEE Transactions on Nanotechnology*, vol. 7, no. 1, pp. 91–99, Jan. 2008.

[19] J. T. Kim and S.-Y. Choi, "Graphene-based plasmonic waveguides for photonic integrated circuits," *Optics express*, vol. 19, no. 24, pp. 24 557–24 562, 2011.

[20] R. G. Cid-Fuentes, J. M. Jornet, E. Alarcon, and I. F. Akyildiz, "A receiver architecture for pulse-based electromagnetic nanonetworks in the terahertz band," in *Proc. of IEEE International Conference on Communications, ICC*, Jun. 2012.

[21] A. Vakil and N. Engheta, "Transformation optics using graphene," *Science*, vol. 332, no. 6035, pp. 1291–1294, Jun. 2011.

[22] R. F. Mills and G. E. Prescott, "A comparison of various radiometer detection models," *Aerospace and Electronic Systems, IEEE Transactions on*, vol. 32, no. 1, pp. 467–473, 1996.